

# Preflare Nonthermal Emission Observed in Microwaves and Hard X-Rays

Ayumi ASAI, Hiroshi NAKAJIMA, and Masumi SHIMOJO

*Nobeyama Solar Radio Observatory, National Astronomical Observatory of Japan, Minamimaki, Minamisaku, Nagano 384-1305*  
asai@nro.nao.ac.jp

Stephen M. WHITE

*Department of Astronomy, University of Maryland, College Park, MD 20742, USA*  
and

Hugh S. HUDSON and Robert P. LIN

*Space Science Laboratory, University of California, Berkeley, CA 94720, USA*

(Received 2005 June 16; accepted 2005 September 29)

## Abstract

We present a detailed examination on nonthermal emissions during the preflare phase of the X4.8 flare that occurred on 2002 July 23. The microwave (17 GHz and 34 GHz) data obtained with the Nobeyama Radioheliograph at Nobeyama Solar Radio Observatory and the hard X-ray data taken with the Reuven Ramaty High Energy Solar Spectroscopic Imager obviously showed nonthermal features in the preflare phase. We also found a faint ejection associated with the flare in the EUV images taken with the Transition Region and Coronal Explorer. We discuss the temporal and spatial features of the nonthermal emissions in the preflare phase, and their relation with the ejection.

**Key words:** Sun: corona — Sun: flares — Sun: particle acceleration — Sun: radio radiation — Sun: X-rays, gamma rays

## 1. Introduction

Nonthermal emissions from accelerated particles are often observed in hard X-rays (HXR),  $\gamma$ -rays, and microwaves at the beginning of a solar flare. These nonthermal emissions are associated with intense energy release processes, which characterize the “impulsive phase” of a flare. The particle acceleration mechanism has been one of the most important and most difficult problems in solar physics (see reviews by, e.g., Aschwanden 2002). As Benz and Grigis (2003) and Lin and RHESSI Team (2003) reported recently, nonthermal emissions are associated with even a small energy release, such as a microflare. However, it has been thought that the particle acceleration mechanism works efficiently only in the impulsive phase.

On the other hand, it is also interesting to study preflare activity, since this may hold the key for understanding how to trigger the catastrophic energy release of the flare. If we identify and understand the preflare signatures, we can anticipate the relevant physical processes of the flare itself. Preflare activity has thus often been studied (e.g., Simnett 1999). In the preflare stage we sometimes find flare-predictive phenomena, such as a gradual enhancement of soft X-ray (SXR) emission, a rise of SXR plasmoids and/or H $\alpha$  filaments, and so on. Even in the preflare stage of a solar flare, some energy release process is probably occurring at a low level, although the energy release is much milder.

However, we have not answered the question whether the energy release at this stage is a scaled-down version of the main flare, as in a microflare, or whether it is totally different. It is not widely accepted that nonthermal particles are present in significant numbers prior to the impulsive phase of a flare; rather, it is common to speak of preflare heating

implying thermal behavior. Therefore, at least in terms of the explosiveness of energy release, the impulsive phase seems to be distinguished from the preflare phase, and reports on nonthermal emissions during the preflare phases have been mostly negative. Fárník et al. (2003) reported the possibility of particle acceleration, even in the preflare phase, although there still remain ambiguities.

Recently, Holman et al. (2003) examined the HXR features of the 2002 July 23 flare, and reported that the nonthermal energy even before the impulsive phase was quite large. Motivated by the work, we analyzed the flare, and found sufficient emissions both in HXR and in microwaves that can be candidates for nonthermal emissions during the preflare phase. Especially, this is the first imaging observation of preflare nonthermal emission in microwaves. In order to derive the information on the energy release in the preflare phase, we examined in detail the features of the emission sources spatially, temporally, and spectroscopically. In this paper we report on the results of investigations of the emissions in HXR and in microwaves during the preflare phase. We also discuss the relation between the nonthermal emissions and other observed phenomena. In section 2 we describe the observational data. In section 3 we examine the detailed features of the nonthermal emissions, dividing the preflare phase into four sub-phases. In section 4 we summarize our results and have discussions.

## 2. Observations and Data

The intense solar flare, which was X4.8 on the GOES scale, occurred in NOAA Active Region 10039 (S12°, E72°) at 00:18 UT, 2002 July 23. This flare showed many spectacular features (e.g., Lin et al. 2003) in HXR and  $\gamma$ -ray

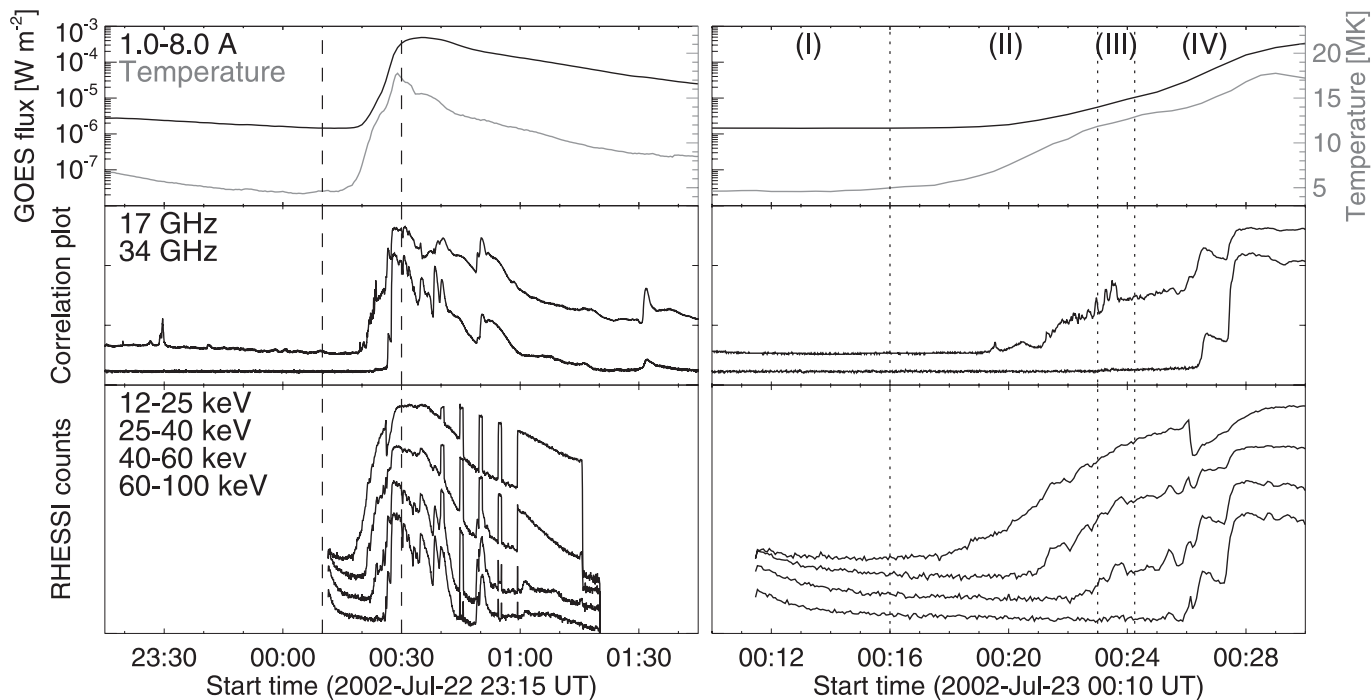


**Fig. 1.** Left: Light curves of the 2002 July 23 flare. From top to bottom: soft X-ray flux in the GOES 1.0–8.0 Å channel (black) and temperature derived from GOES fluxes (gray); radio correlation plot observed at 17 GHz and 34 GHz with NoRH (scaled arbitrarily); hard X-ray count rate measured with RHESSI in four bands (12–25 keV, 25–40 keV, 40–60 keV, and 60–100 keV; scaled arbitrarily). Two dashed vertical lines show the time range of the preflare phase. Right: Light curves of the preflare phase. Three dotted vertical lines divide the preflare phase into four sub-phases as numbered.

wavelengths obtained with the Reuven Ramaty High Energy Solar Spectroscopic Imager (RHESSI; Lin et al. 2002). This flare was also observed in microwaves with the Nobeyama Radioheliograph (NoRH; Nakajima et al. 1994), as reported by White et al. (2003). In this paper we focus on the nonthermal emissions in HXRs and in microwaves of the preflare phase, from about 23:00 UT, 2002 July 22 to about 00:30 UT, 2002 July 23. The left panel of figure 1 shows time profiles of the flare in SXR, microwaves, and HXRs. The top two lines are the GOES 1.0–8.0 Å channel (black line) and the temperature profile (gray line), the middle ones are in NoRH 17 GHz and 34 GHz, and the bottom ones are the RHESSI time profiles in four energy ranges of 12–25 keV, 25–40 keV, 40–60 keV, and 60–100 keV. We divide the preflare phase into four sub-phases, and examine each phase in more detail in the following sections. The right panels of figure 1 show the expanded light curves of the preflare phase of the flare (from 00:10 UT to 00:30 UT, 2002 July 23), which corresponds to the time between the dashed lines in the left panel. The time ranges of the four sub-phases are numbered at the top of the right panel of figure 1.

NoRH observes the Sun in two frequencies, 17 GHz and 34 GHz, which allow us to derive a spectral index,  $\alpha$  ( $F_\nu \propto \nu^\alpha$ ;  $F_\nu$  is the flux at frequency  $\nu$ ), with a temporal resolution of 1 s. The spatial resolutions (FWHMs) of NoRH data are 14'' for 17 GHz and 7'' for 34 GHz. We synthesized the HXR images obtained with RHESSI by using grids 4–8 which give the spatial resolution (FWHM) of about 12''. We integrated over 20 s to synthesize each image in this paper. We also measured the temperature and the emission measure of the

thermal plasma in the corona by using the ratios of the two of GOES channels. We plotted the time profiles of the temperature derived from GOES in the top panels of figure 1. EUV images of the flare were obtained with the Transition Region and Coronal Explorer (TRACE; Handy et al. 1999; Schrijver et al. 1999). We used 195 Å images, in which the Fe XII line formed at  $\sim 1$  MK is normally dominant. The pixel size of the CCD is 1''0, and the temporal resolution is about 9 s.

### 3. Results

#### 3.1. Phase I: Before the Flare

This phase corresponds to the time from about 23:30 UT, 2002 July 22 to 00:16 UT, 2002 July 23. Figure 2 shows images of the flare for each phase. The left panels show the TRACE 195 Å images overlaid with the contour images of the NoRH 34 GHz (red), the RHESSI 25–40 keV (yellow), and the 40–60 keV (blue, only in the bottom panel), respectively. The right panels show the maps of NoRH  $\alpha$  index overlaid with the RHESSI 12–25 keV intensity (white). We can see a large loop-like bright region in the NoRH image (White et al. 2003). We measured the spectral index,  $\alpha$ , of the emission source, and found that it is about 0 (within range of  $-0.4$  to  $0.6$ ). Therefore, the optically thin (free-free) thermal emission is dominant for the source. Moreover, the polarization of the sources is no more than 10%, which eliminates the possibility of emission from the gyroresonance near sunspot umbrae. To confirm this, we also estimated the microwave fluxes in 17 and in 34 GHz from the temperature and the emission measure, which were derived from GOES, and found that the estimated fluxes were

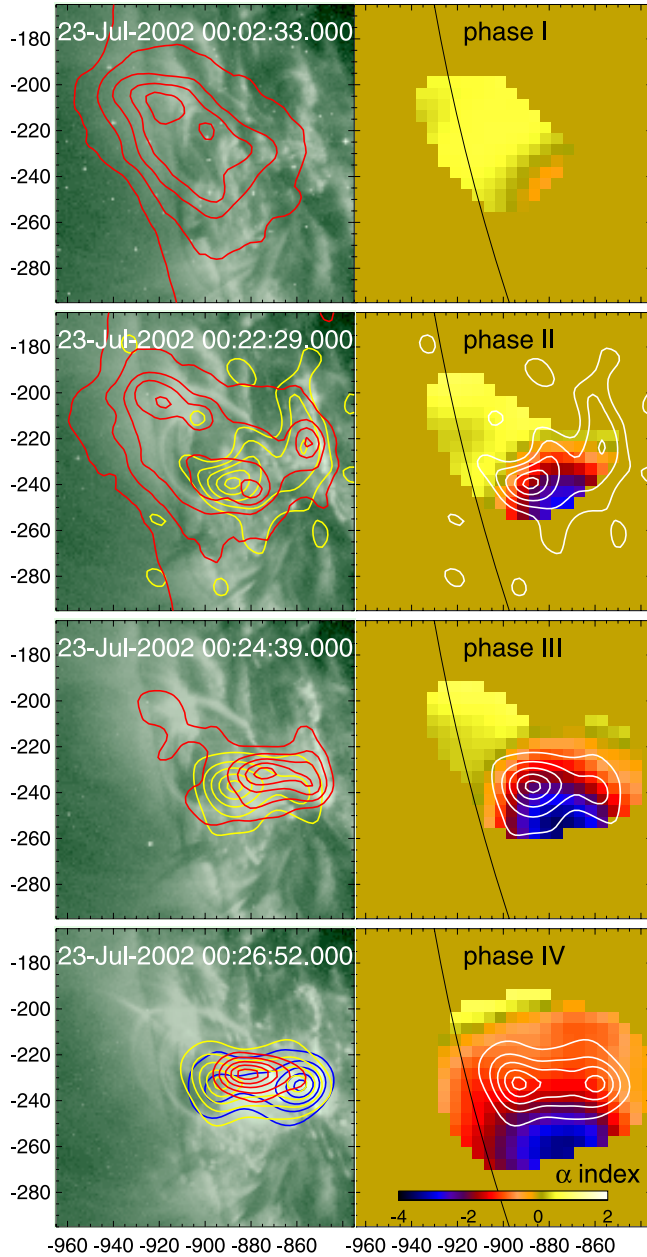


**Fig. 2.** Images of the flare for each phase. Solar north is up, and west is to the right. The left panels show the EUV images taken with TRACE 195 Å. The contours show the NoRH 34 GHz brightness temperature (red), the RHESSI 25–40 keV intensity (yellow), and the 40–60 keV intensity (blue, only in the bottom panel), respectively. The right panels show the maps of NoRH  $\alpha$  index overlaid with the RHESSI 12–25 keV intensity (white). The 34 GHz contours are 15, 30, 50, 70, and 90% of the peak intensity. Contours for the RHESSI HXR images are at 20, 40, 60, 80, and 95% of the peak intensity.

almost the same as the observed ones. We defined the emission from the background corona as the average emission between 20:30 UT and 21:10 UT on 2002 July 22.

The GOES temperature shows the existence of hot plasma even in this phase of about 5 MK (see the top panels of figure 1). This could be related to a small flare that occurred at 22:00 UT in the same active region, although we could not

confirm this due to a lack of image data for the small event. It was at a time before NoRH started observations, and RHESSI was unavailable due to the SAA and the night. Although TRACE was observing the region, we could not see any active phenomena at the time. This is presumably because the large structure is too hot to be observed in the EUV range. In any case, we could not see any signs of triggering the flare in this phase.

### 3.2. Phase II: Preflare Phase

This phase includes the first flare emissions (from 00:16 UT to 00:23 UT). We can see some thermal emission features and also clear signatures of nonthermal emission. This phase is the most important one for this paper.

First, we summarize the features of the time profiles. The GOES temperature rapidly increases from about 4.5 MK at 00:15 UT to above 10 MK at 00:22 UT. At the same time, the RHESSI count rate in 12–25 keV increases as shown in figure 1. Such HXR brightenings in lower energy bands, associated with a hotter GOES source, are often observed in a preflare phase, and the emissions are thought to be thermal. Holman et al. (2003) performed a spectroscopic analysis of the flare with RHESSI data, and reported that the thermal component of the region has high temperature up to 20–30 MK. After some short delay, from 00:18 UT the NoRH 17 GHz emission starts to rise, and the temporal evolution resembles the RHESSI 25–40 keV light curve. The NoRH 34 GHz emission and the RHESSI 40–60 keV count rate start to rise at 00:22 UT almost simultaneously.

Here, we summarize the spatial features of the emission sources. The panels in the second row from the top of figure 2 show images of the phase taken at 00:22:30 UT. In the TRACE images, we can see that a large two-ribbon structure (White et al. 2003) brightens from 00:20 UT. The brightening of the ribbons implies that a larger structure rather than the core of the flare destabilizes in this phase. In figure 3 we present enlarged images that show the spatial features. The TRACE EUV images in the left and the middle panels were taken a few minutes after this phase. We can see a diffuse loop-like structure that is identified as Fe XXIV emission from 20 MK plasma, as is often observed in TRACE 195 Å images during flares. A new microwave source appears above the flare ribbons at (−878, −243) arcsec heliocentric. This site corresponds to the post flare loops, which become visible in the later phase in the TRACE images and which connect the flare ribbons. The  $\alpha$  index is about −3.0, which implies that this source is emitting nonthermal-gyrosynchrotron radiation. The index is quite small and shows a steep (soft) power-law spectrum. An HXR source also appears at this site, although it is apparently slightly higher (−890, −240) than the microwave emission source. Figure 3 shows the HXR source to be at the top of the diffuse TRACE loop. The HXR source is visible in both the 12–25 keV and 25–40 keV bands. These sources could resemble the “loop-top” HXR source (Masuda et al. 1994). On the other hand, we can also see footpoint sources that are located on the TRACE flare ribbons mentioned above both in the microwave (34 GHz) and in the HXR (12–25, 25–40 keV). The energy release probably occurs in the corona, some part of which is deposited at the footpoints to produce the EUV

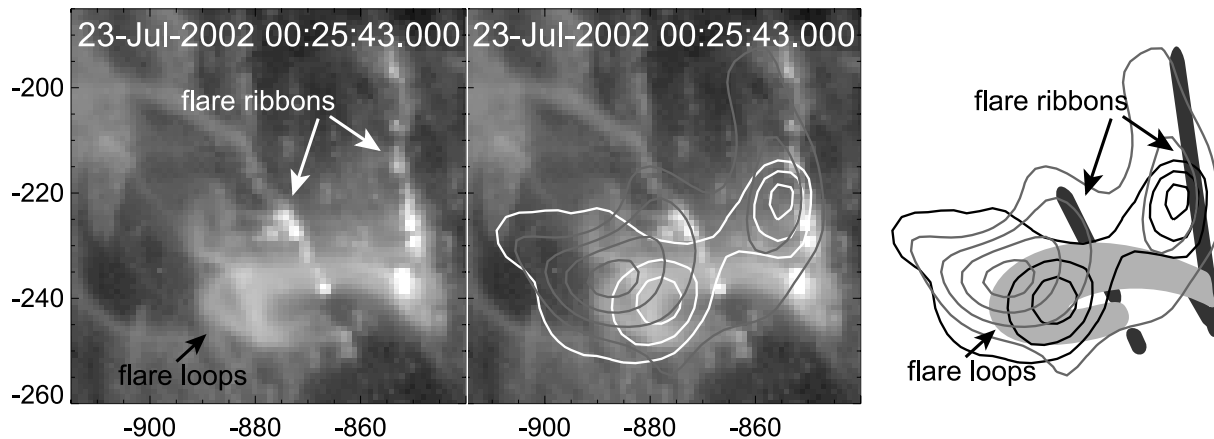


**Fig. 3.** Spatial distribution of the emission sources. Solar north is up, and west is to the right. The left and the middle panels show EUV images taken with TRACE 195 Å. The contours in the middle and the right panels show the NoRH 34 GHz brightness temperature (white in the middle and black in the right), and the RHESSI 25–40 keV intensity (gray), respectively. The right panel also shows the positions of the flare ribbons (dark gray regions) and the flare loops (light gray).

brightenings. The HXR emissions from the flare ribbon are thought to be generated by thick-target emission by nonthermal electrons. This is evidence for the existence of the nonthermal particles in this phase.

### 3.3. Phase III: Ejection

Next, we focus on the small microwave burst and the faint EUV ejection that occurred at about 00:23:30 UT. In figure 4 we show the relationship between the timing of the EUV ejection and the nonthermal microwave emission. The arrows indicate the time when the ejection started. The projected speed of the ejection on the time slice image is roughly about  $250 \text{ km s}^{-1}$ . A halo coronal mass ejection (CME) associated with the flare was also observed with Large Angle Spectrometric Coronagraph (LASCO) on board the Solar and Heliospheric Observatory (SOHO: see the SOHO/LASCO CME online catalog;<sup>1</sup> Yashiro et al. 2004). A combination of ejections and HXR bursts has been observed in impulsive flares (Kano 1994; Hudson et al. 1996; Ohyama, Shibata 1997), and is consistent with the “plasmoid-induced reconnection model” (Shibata 1999). The plasmoid ejections correspond in detail with nonthermal emissions, and CME acceleration may also show this pattern (e.g., Zhang et al. 2001).

The NoRH 34 GHz source moved slightly northward ( $-875, -230$ ), and showed a loop-like structure. This loop structure corresponds to the most intense post-flare loop, which appeared later in the TRACE 195 Å images. The HXR RHESSI 12–25 keV and 25–40 keV emissions still appear at the top of the NoRH loop. Although the source positions moved northward as to the 34 GHz emission, they could not be identified because of limitations of the spatial resolution.

### 3.4. Phase IV: Impulsive Phase

This phase corresponds to the time after the TRACE ejection and before the start of the impulsive phase (from 00:24 UT to 00:27 UT). Approximately speaking, the physical features are the same as in the impulsive phase, as Krucker, Hurford, and

Lin (2003) reported. The positions of the emission sources do not change so much from the previous phase, III. The HXR coronal sources ascend slightly as the flare progresses. The 34 GHz emission gradually comes to localize on the upper section of the loop. As a notable result, we can see an HXR loop-top source even in 40–60 keV as shown in the bottom-left panel of figure 2. In this phase, the  $\alpha$  index increases slightly (becomes harder) to about  $-1.5$ .

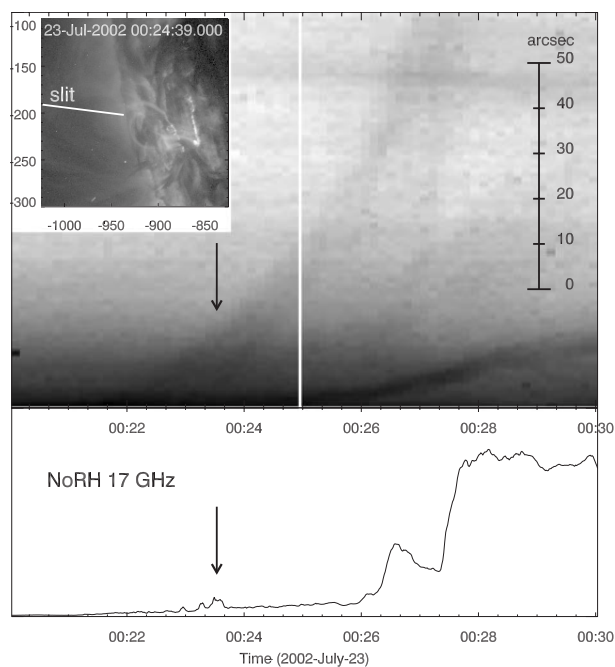


**Fig. 4.** Top left: an EUV image of the flare observed with TRACE. The white solid line illustrates the position of the slit line. Top right: time-sequenced EUV (195 Å) image (time slice image) obtained with TRACE along the slit line. The horizontal and the vertical axes are time (UT) and the space along the slit, respectively. Bottom: microwave (17 GHz) light curve obtained with NoRH.

<sup>1</sup> See ([http://cdaw.gsfc.nasa.gov/CME\\_list/](http://cdaw.gsfc.nasa.gov/CME_list/)).

#### 4. Discussion and Summary

In this paper, we examined in detail the nonthermal emissions in the preflare phase spatially, temporally, and spectroscopically. We also examined the relation between the nonthermal emissions and other observed phenomena. We identified a faint EUV ejection in the TRACE data, which was associated with a nonthermal microwave burst, just before the fast energy release process occurs in the impulsive phase. In the phase before the ejection, we found observational evidence of both thermal and nonthermal emissions in the corona above the flare ribbon structure.

Under the standard reconnection model, the current sheet reduces its thickness in the preflare phase (Magara, Shibata 1999), which leads to fast magnetic reconnection and a violent energy release in the impulsive phase. This process

is associated with the slow reconnection and/or the low-level energy release, and leads to heating the coronal plasma, as often observed. Our results, on the other hand, indicate that the process also releases enough energy under the right conditions to accelerate particles to nonthermal energies. This suggests that the energy release mechanism in the preflare phase of a typical flare may be accompanied by particle acceleration, although it is much milder than that in the impulsive phase, and therefore hardly detected in flares smaller than this event.

We first acknowledge an anonymous referee for his/her useful comments and suggestions. We wish to thank Drs. G. D. Holman and L. Sui for fruitful discussions and their helpful comments. We made extensive use of TRACE and RHESSI Data Center.

#### References

- Aschwanden, M. J. 2002, *Space Sci. Rev.*, 101, 1  
 Benz, A. O., & Grigis, P. C. 2003, *Adv. Space Res.*, 32, 1035  
 Fárník, F., Hudson, H. S., Karlický, M., & Kosugi, T. 2003, *A&A*, 399, 1159  
 Handy, B. N., et al. 1999, *Sol. Phys.*, 187, 229  
 Holman, G. D., Sui, L., Schwartz, R. A., & Emslie, A. G. 2003, *ApJ*, 595, L97  
 Hudson, H. S., Acton, L. W., & Freeland, S. L. 1996, *ApJ*, 470, 629  
 Kano, R. 1994, in *X-Ray Solar Physics from Yohkoh*, ed. Y. Uchida, T. Watanabe, K. Shibata, & H. S. Hudson (Tokyo: Universal Academy Press), 273  
 Krucker, S., Hurford, G. J., & Lin, R. P. 2003, *ApJ*, 595, L103  
 Lin, R. P., et al. 2002, *Sol. Phys.*, 210, 3  
 Lin, R. P., et al. 2003, *ApJ*, 595, L69  
 Lin, R. P., & RHESSI Team 2003, *Adv. Space Res.*, 32, 1001  
 Magara, T., & Shibata, K. 1999, *ApJ*, 514, 456  
 Masuda, S., Kosugi, T., Hara, H., Tsuneta, S., & Ogawara, Y. 1994, *Nature*, 371, 495  
 Nakajima, H., et al. 1994, *Proc. IEEE*, 82, 705  
 Ohya, M., & Shibata, K. 1997, *PASJ*, 49, 249  
 Schrijver, C. J., et al. 1999, *Sol. Phys.*, 187, 261  
 Shibata, K. 1999, *Ap&SS*, 264, 129  
 Simnett, G. M. 1999, in *The Many Faces of the Sun*, ed. K. T. Strong, J. L. R. Saba, B. M. Haisch, & J. T. Schmelz (New York: Springer-Verlag), 201  
 White, S. M., Krucker, S., Shibasaki, K., Yokoyama, T., Shimojo, M., & Kundu, M. R. 2003, *ApJ*, 595, L111  
 Yashiro, S., Gopalswamy, N., Michalek, G., St. Cyr, O. C., Plunkett, S. P., Rich, N. B., & Howard, R. A. 2004, *J. Geophys. Res.*, 109, A07105  
 Zhang, J., Dere, K. P., Howard, R. A., Kundu, M. R., & White, S. M. 2001, *ApJ*, 559, 452

